Ab Initio Molecular Orbital Calculations for the N(^{2}D) + Ethylene Reaction

Toshiyuki Takayanagi* and Yuzuru Kurosaki

Advanced Science Research Center, Japan Atomic Energy Research Institute, Tokai-mura, Naka-gun, Ibaraki 319-1195, Japan

Kei Sato and Shigeru Tsunashima

Department of Applied Physics, Faculty of Science, Tokyo Institute of Technology, Ookayama, Meguro-ku, Tokyo 152-8551, Japan

Received: June 30, 1998; In Final Form: September 14, 1998

The lowest doublet potential energy surface for the N(^{2}D) + C_2H_4 reaction has been characterized using ab initio molecular orbital theory. The CASSCF/cc-pVDZ calculations predict that the dominant mechanism is the addition of N(^{2}D) to the CC π-bond of C_2H_4 to form a cyclic three-membered intermediate radical rather than the insertion into the CH bond in C_2H_4. Reaction pathways have also been discussed on the basis of the PMP4(full,SDTQ)/cc-pVTZ//MP2/cc-pVDZ level calculations. The reaction is shown to have several possible products via somewhat complicated reaction mechanisms. The results of RRKM calculations predict that the main product channel is cyclic-CH(N)CH_2 (azirine) + H under collision-free conditions.

Introduction

The reactions of N atoms with hydrocarbons have been traditionally studied using so-called active nitrogen,[1,2] which is the mixture of ground- and excited-state atomic and molecular nitrogen. Despite the fact that active nitrogen includes many reactive species such as a metastable nitrogen atom N(^{2}D) or N(^{2}P) and an excited nitrogen molecule $N_2(^3\Sigma_u^+)$, these early experiments[1,2] assume that the only reactive species are ground-state nitrogen atoms N(^{4}S). Therefore, the reaction mechanisms for N atoms with hydrocarbons, speculated on the basis of the early product analysis studies, must be somewhat ambiguous. Later, rate-constant measurements for the reactions of the N atoms with various hydrocarbons were carried out, in which the electronic state of the N atom was identified using spectroscopic techniques. For example, Fell et al.[3] employed an electron-spin-resonance technique to measure rate constants of N(^{2}D) with various molecules. Umemoto et al.[4] used a pulse radiolysis-resonance absorption technique to determine rate constants of N(^{2}P) with molecules. These kinetic studies gave important information beyond early product analysis results using active nitrogen; however, kinetic studies are not able to identify the primary reaction products, since they follow the decay of the N atom.

Very recently, two research groups have developed sophisticated experimental techniques which open up the possibility of studying the reactions of the N(^{2}D) atom under single-collision conditions. The first one is a laser photolysis technique by Umemoto and co-workers,[5] in which the N(^{2}D) atom is efficiently produced from NO via two-photon dissociation. This technique has been applied to the N(^{2}D) + H_2, CH_4, C_2H_6, and C_3H_8 reactions, and nascent quantum state distributions of the NH product were determined.[6−8] The other is the crossed molecular beam technique by Casavecchia and co-workers.[9] They succeeded in generating intense supersonic beams of the N(^{2}D) atom and applied those to the N(^{2}D) + H_2 and C_2H_2 reactions.[10,11] They have obtained dynamical information including angular and translational energy distributions of reaction products.[10,11]

In addition to the development of the experimental techniques mentioned above, theoretical calculations using ab initio molecular orbital (MO) theory also play important roles in understanding overall reaction mechanisms as well as in interpreting experimental results. In particular, we can obtain accurate reaction energy diagrams including all possible products within an error of several kilocalories per mole using modern electronic structure theory with large basis sets. We have previously reported ab initio calculations on the potential energy surfaces for the reactions of N(^{2}D) with H_2, CH_4, and C_2H_2.[12−14]

In this paper we present ab initio MO calculations of the potential energy surface for the reaction of the N(^{2}D) atom with ethylene. Although the N(^{2}D) + C_2H_4 reaction is very simple, experimental information is very limited; the available information is only for the rate constant at room temperature.[3] However, crossed molecular beam experiments are currently undertaken by Casavecchia and co-workers.[11] Also, our research group is currently measuring the temperature dependence of the rate constants for N(^{2}D) + C_2H_4 and C_2D_4.[15] Therefore, it is quite meaningful to report theoretical information on the potential energy surface for N(^{2}D) + C_2H_4. In addition, it would be very interesting to compare the reaction mechanisms for N(^{2}D) + C_2H_4 with those for N(^{2}D) + CH_4 and C_2H_2. Our previous studies[13,14] have revealed that N(^{2}D) inserts into the C−H bond in CH_4 while N(^{2}D) adds to the π-bond in C_2H_2. In the case of N(^{2}D) + C_2H_4, both addition to the π-bond and insertion into the C−H bond are possible.

Another important issue which should be addressed is that of main reaction products. If N(^{2}D) adds to the CC π-bond in C_2H_4, a cyclic intermediate radical is primarily produced. Also, if N(^{2}D) inserts into the CH bond, an intermediate radical, CH_2=CHNH, may be formed. Thus, the reaction products of the N(^{2}D) + C_2H_4 reaction may be essentially the same as the dissociation products of these intermediate radicals. However, to understand

* Author to whom correspondence should be addressed.

10.1021/jp982811j CCC: $15.00
Published on Web 11/18/1998

the overall reaction pathways, additional information is required on the isomerization pathway between these intermediates as well as an isomerization barrier height.

Here, we investigate the detailed characteristics of the lowest doublet potential energy surface for the $N(^2D) + C_2H_4$ reaction using ab initio MO theory. Reaction mechanisms and possible product channels are discussed on the basis of the computational results.

Computational Procedure

All ab initio calculations presented in this paper were performed using the Gaussian 94 program package.[16] Two different electronic structure methods were used in this study: the complete-active-space self-consistent-field (CASSCF) method and the Møller−Plesset (MP) perturbation method using the Hartree−Fock (HF) wave functions.

The CASSCF method was employed to understand whether the $N(^2D) + C_2H_4$ reaction is additive or insertive. Since atomic nitrogen has three electrons on the 2p orbital, the electronic configuration of $N(^2D)$ can roughly be expressed as $(2p)^{\uparrow}(2p)^{\uparrow}(2p)^{\downarrow}$. This means that the electronic structure of $N(^2D)$ cannot be described by the single-determinant HF theory. In fact, if we employ the unrestricted HF theory for $N(^2D)$, the wave function was affected by a considerable amount of spin contamination. The basis set used was the correlation-consistent polarized valence double-ζ (cc-pVDZ) of Dunning.[17] Five active orbitals were employed: three nitrogen 2p orbitals, CC π- and CC π^*-orbitals in C_2H_4. Five electrons were distributed among these five orbitals (denoted as CASSCF(5,5)/cc-pVDZ). Saddle point structures were fully optimized at this CASSCF(5,5)/cc-pVDZ level. The harmonic vibrational frequencies were also calculated at the same level in order to characterize the optimized geometries as saddle points.

The Møller−Plesset perturbation method was used to calculate the reaction energy diagram and thus to understand possible product channels. The geometries of the reactants, products, intermediates, and transition states have been fully optimized at the second-order Møller−Plesset (MP2) level of theory with the cc-pVDZ basis set. Harmonic vibrational frequencies were calculated at the same level in order to characterize the optimized geometries as potential minima or saddle points. Single-point calculations for the MP2/cc-pVDZ geometries were also carried out using the spin-projected fourth-order MP method including single, double, triple, and quadruple substitutions (denoted as PMP4(SDTQ)) with the correlation-consistent polarized valence triple-ζ (cc-pVTZ)[17] basis set in order to obtain more accurate energy values. All electrons were included in all the MP calculations.

Results and Discussion

A. Reaction Mechanisms: Addition vs Insertion: The transition-state geometries for addition and insertion optimized at the CASSCF/cc-pVDZ level of theory are shown in Figure 1. These are referred to as TS_{add} and TS_{ins}, respectively. The total energies and harmonic vibrational frequencies are summarized in Tables 1 and 2, respectively. It has been found that TS_{add} and TS_{ins} have C_{2v} and C_1 symmetry, respectively. The intrinsic-reaction-coordinate (IRC) calculations were also carried out to confirm that TS_{add} and TS_{ins} are true saddle points for the addition and insertion reactions, respectively. It was found that TS_{add} is smoothly connected to the structure of the cyclic intermediate radical M_1 (defined in the next section). Also, TS_{ins} was smoothly connected to the intermediate radical $CH_2{=}CHNH$ (M_3 defined in the next section).

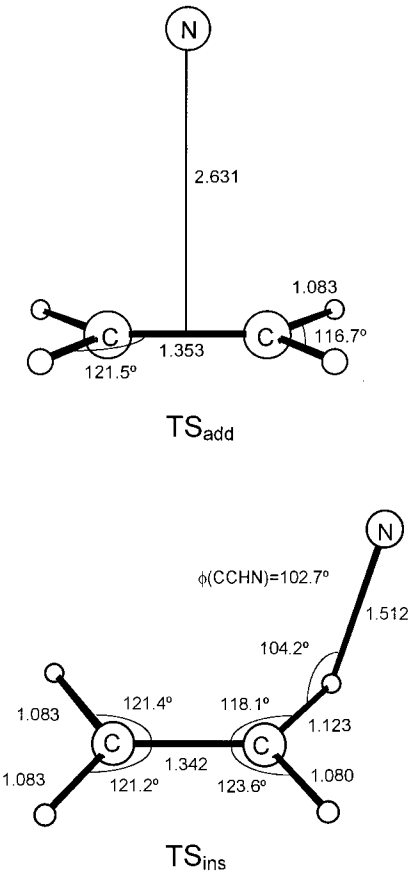

Figure 1. Molecular geometries of the transition states (saddle points) for the $N(^2D) + C_2H_4$ reaction calculated at the CASSCF(5,5)/cc-pVDZ level of theory. TS_{add} is the transition state for addition, and TS_{ins} for insertion.

TABLE 1: Total Energies Calculated at the CASSCF/cc-pVDZ Level

	energy/au	symmetry
$N(^2D)$	−54.28272	
$C_2H_4(^1A_g)$	−78.06793	D_{2h}
$TS_{add}(^2B_1)$	−132.34552	C_{2v}
$TS_{ins}(^2A)$	−132.32997	C_1

TABLE 2: Harmonic Vibrational Frequencies Calculated at the CASSCF/cc-pVDZ Level

molecule	vibrational frequencies/cm^{-1}
C_2H_4	843(b_{2g}), 876(b_{2u}), 924(b_{3u}), 1079(a_u), 1319(b_{3g}), 1425(a_g), 1562 (b_{1g}), 1751(a_g), 3285(b_{1u}), 3306(a_g), 3370(b_{3g}), 3397(b_{2u})
TS_{add}	349i(a_1), 129(b_2), 203(b_1), 837(b_2), 873(b_1), 902(a_1), 1037(a_2), 1317(a_2), 1335(a_1), 1561(b_2), 1667(a_1), 3295(b_2), 3305(a_1), 3383(a_2), 3410(b_1)
TS_{ins}	554i, 173, 367, 849, 864, 951, 1116, 1263, 1378, 1498, 1707, 2741, 3304, 3381, 3404

For the structure of TS_{add}, the distance between the N atom and the center of mass of C_2H_4 was calculated to be 2.63 Å. Also, from Table 2 it is seen that the difference in vibrational frequencies between TS_{add} and the reactant C_2H_4 is very small (<100 cm^{-1}). These results qualitatively indicate that the addition reaction of $N(^2D)$ to C_2H_4 can be classified to have an early saddle point. On the other hand, it is also interesting to note that the saddle point structure for insertion, TS_{ins}, is very similar to that for the $N(^2D) + CH_4$ insertion reaction,[13] which

was previously reported. In the case of N(^{2}D) + CH_4, the internuclear distance between N and H was calculated to be 1.516 Å,[13] which is comparable to the present result, 1.512 Å.

The classical barrier height for addition of N(^{2}D) is estimated to be 3.2 kcal/mol from the total energies calculated at the CASSCF(5,5)/cc-pVDZ level listed in Table 1. On the other hand, the barrier height for insertion of N(^{2}D) is calculated to be 13.0 kcal/mol at the same level of theory, which is 9.8 kcal/mol larger than addition. However, this result is only qualitative since the active space employed does not include the CH σ- and σ*-orbitals. Therefore, we have carried out the single-point CASSCF(7,7) calculations including the highest CH σ- and lowest CH σ*-orbitals, and two more electrons. The calculated energy difference was 7.3 kcal/mol, indicating that the barrier height for addition is still smaller than that for insertion. Consequently, it may be expected that the insertion mechanism can safely be ignored for usual thermal conditions, although a more accurate electronic structure theory such as multireference configuration interaction (MRCI) method would be needed to obtain more accurate values of the barrier heights for addition and insertion. This is simply because the CASSCF method does not include the dynamical electron correlation effect, which is generally important for accurate estimation of reaction barrier heights.

Although the barrier height for addition of N(^{2}D) to C_2H_4 calculated at the CASSCF level is not reliable, it may be informative to compare the transition-state theory (TST) rate constant with the available experimental rate constant. The TST rate constant, k(T), can be expressed as

$$k(\mathrm{T}) = Lg_{\mathrm{e}}\frac{k_{\mathrm{B}}T}{h}\frac{Q^{\ddagger}}{Q_{\mathrm{r}}}\mathrm{e}^{-E_0/k_{\mathrm{B}}T}$$

where k_B and h are Boltzmann's constant and Planck's constant, respectively. L is the reaction path degeneracy and is 2 for the addition reaction. E_0 is the barrier height including the zero-point vibrational energy correction. $Q^{\ddagger}$ and Q_r are the partition functions for the transition state and reactant, respectively. Note that the partition functions do not include the contribution of electronic states. Instead, we employ an additional factor g_e which takes the contribution of electronic degeneracy into account (referred to as "multiple surface coefficient" in ref 21). If we assume that only the lowest doublet potential energy surface is reactive and the reaction adiabatically proceeds on this surface, g_e becomes 0.2 since the electronic state of N(^{2}D) is 5-fold degenerate without spin−orbit interactions. On the other hand, if the nonadiabatic transition processes among the five potential energy surfaces are very fast, g_e approximately becomes unity. We here assume that g_e is not temperature dependent for simplicity.

First, we consider only the $g_e = 0.2$ case. As mentioned previously, the rate constant for N(^{2}D) + C_2H_4 has been measured to be 8.3×10^{-11} cm^3 molecule^{-1} s^{-1} at room temperature by Fell et al.[3] If we apply the CASSCF/cc-pVDZ barrier height of 3.2 kcal/mol and employ the vibrational frequencies listed in Table 2, the rate constant at 300 K is calculated to be 1.2×10^{-14} cm^3 molecule^{-1} s^{-1}, which is much smaller than the experimental value by a factor of about 7000. This is not surprising since the ab initio barrier height at the CASSCF level is not accurate. However, if we assume the barrier height to be zero, the TST rate constant at 300 K is 3.0×10^{-12} cm^{3}molecule^{-1} s^{-1}, which is still smaller than the experimental value by a factor of about 27. One of the possible reasons for this serious disagreement is that the saddle point

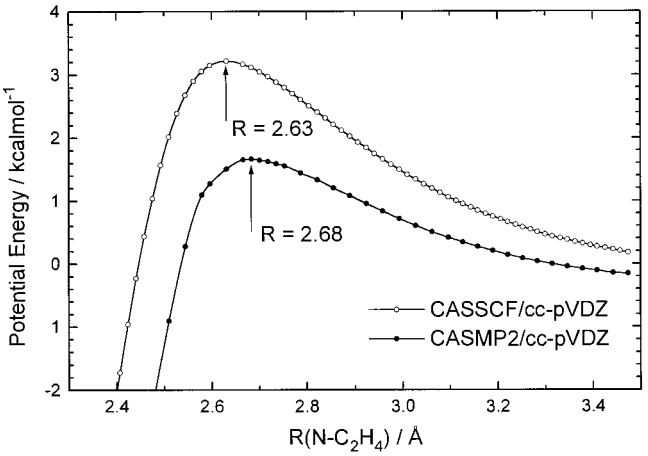

Figure 2. IRC potential energy profile as a function of the internuclear distance between N and the midpoint of CC in C_2H_4. The arrow indicates the location of the potential maximum at each level of theory.

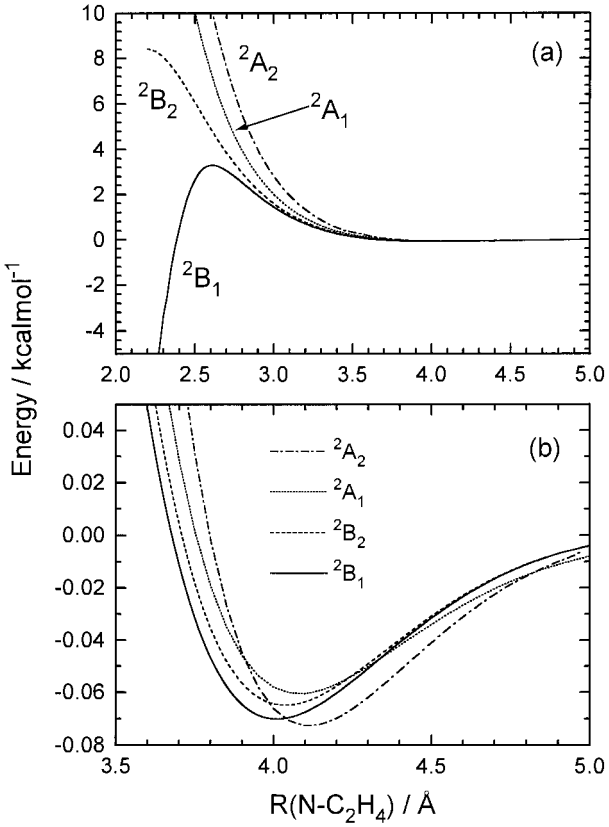

Figure 3. (a) Potential energy curves as a function of the distance between N and the center of mass of C_2H_4 for the lowest four doublet states calculated at the CASSCF(5,5)/cc-pVDZ level. (b) Expansions of the potential energy curves in an asymptotic van der Waals region.

properties for the addition reaction of N(^{2}D) to C_2H_4 calculated at the CASSCF/cc-pVDZ level are not accurate. In fact, it is generally known that the location of the saddle point strongly depends on the ab initio level of theory for the reaction having a very small barrier.[18]

To confirm the possibility that the location of the saddle point depends on the level of theory, it would be better to optimize the saddle point geometry at a more accurate ab initio level of theory such as MRCI although this is computationally prohibitive. Instead, we have carried out CASMP2[19] calculations along the CASSCF IRC path. Figure 2 shows the potential energies along the CASSCF IRC path. Note that the energies are plotted as a function of the internuclear distance between N and C_2H_4.

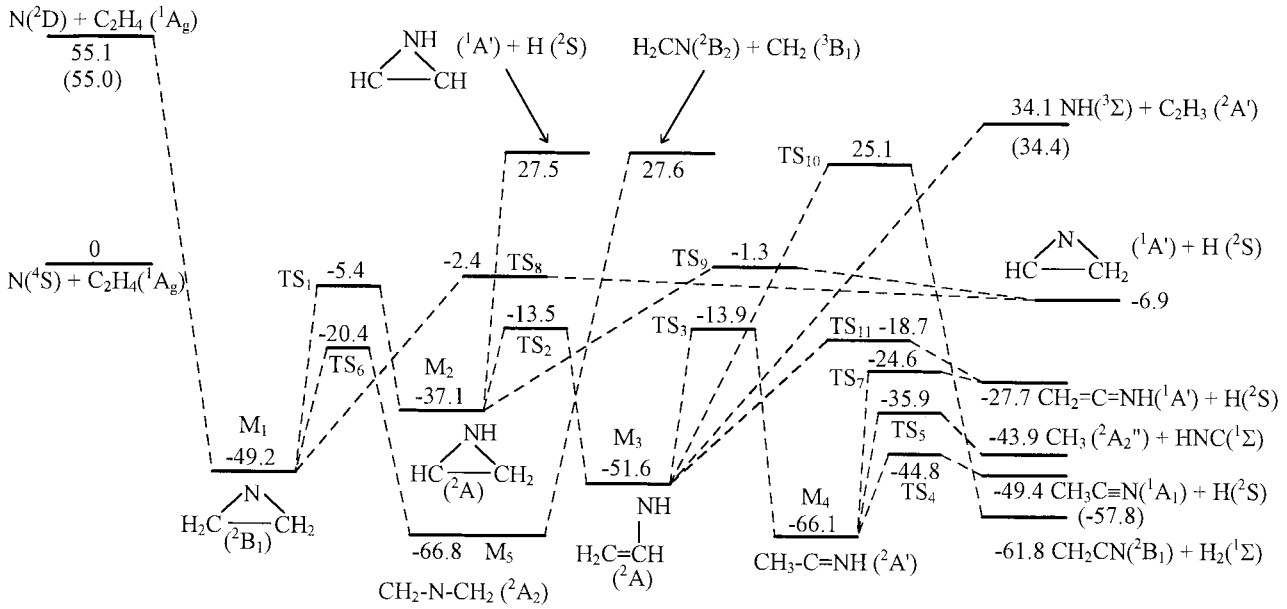

Figure 4. Schematic energy diagram (in kcal/mol) for the N(^{2}D) + C_2H_4 reaction at the PMP4(SDTQ)/cc-pVTZ//MP2/cc-pVDZ level of theory. The energy of the N(^{4}S) + C_2H_4 reactants is defined to be zero.

The zero of energy is the energy of the N(^{2}D) + C_2H_4 reactants at each level of theory. As expected, it is apparently noted that the CASMP2 calculations significantly reduce the barrier height (1.6 kcal/mol) and at the same time shift the location of the potential maximum toward the reactant side. If the true saddle point occurs at a longer distance than the CASSCF value, it is expected that the corresponding vibrational frequencies and rotational constants at the transition state should be smaller than the CASSCF results. To study the sensitivity of the absolute values of the vibrational frequencies and rotational constants on the rate constants, we reduced the frequencies and rotational constants at the transition state by 20%. The TST rate constant at 300 K thus calculated is 1.0×10^{-12} cm^3 molecule^{-1} s^{-1} even with the barrier height being zero. This value is still smaller than the experimental value by a factor of 8. Therefore, we have to employ unphysically small values for the vibrational frequencies and rotational constants in order to reproduce the experimental rate constant within the TST approximation.

In the above TST calculations, we assumed $g_e = 0.2$; i.e., the reaction adiabatically occurs on the lowest doublet potential energy surface. Here, the validity of this assumption should be discussed. Although the importance of nonadiabatic transitions in asymptotic regions was suggested some years ago,[20−22] it is still difficult to discuss this point quantitatively. This is because information on all excited-state potential energy surfaces coupled to a reactive surface and on absolute values of nonadiabatic transition probabilities among these surfaces is necessary. Therefore, we qualitatively consider the contribution of nonadiabatic transitions on the basis of limited information on potential energy curves. Figure 3 shows the potential energy curves of the lowest four doublet states calculated at the CASSCF(5,5)/cc-pVDZ level as a function of R, which is the distance between N and the center of mass of C_2H_4. In these calculations only a perpendicular approach of N to the molecular plane of C_2H_4 was examined, meaning that the molecular geometries are within C_{2v} symmetry. Also, the geometry of C_2H_4 remained unchanged. From Figure 3a it can be seen that the lowest $^2B_1$ state is reactive with a small barrier height; however, these four states are very close in energy in the asymptotic region. Expansions of these four potential curves in the asymptotic region are shown in Figure 3b. Very shallow van der Waals wells are seen around $R = 4$ Å for all the four states. Interestingly, we can see several crossing points around this van der Waals region. This result indicates that there are many avoided crossing points in this region once the molecular geometry reduces to C_1 symmetry. Also, this strongly suggests that nonadiabatic transitions are significant in this region. Therefore, it is expected the factor g_e should be much larger than 0.2 for the N(^{2}D) + C_2H_4 reaction. This behavior was also predicted in our previous study[14] on the N(^{2}D) + C_2H_2 reaction, in which the measured rate constants are much larger than the TST calculations with $g_e = 0.2$. Although the CASSCF level calculations are not very accurate and our discussion is only qualitative, it should be emphasized that nonadiabatic transitions

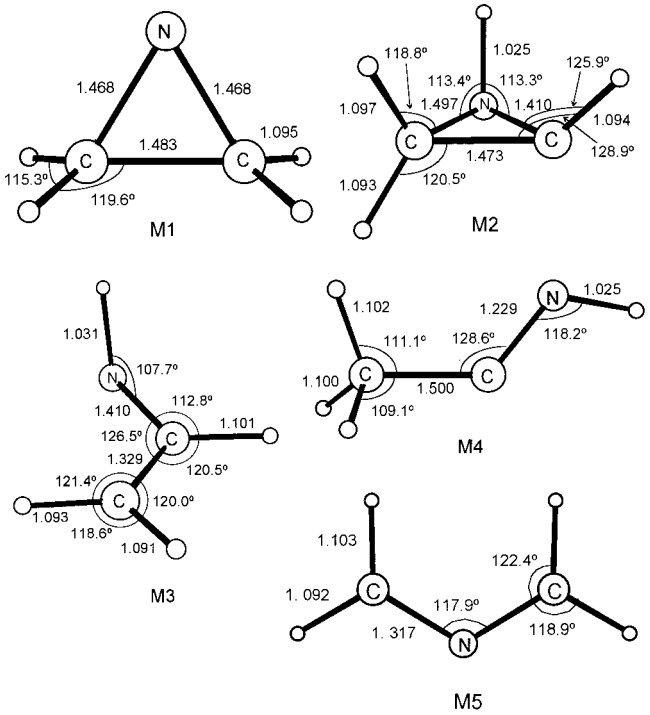

Figure 5. Molecular geometries of the intermediates on the lowest doublet potential energy surface for N(^{2}D) + C_2H_4 optimized at the MP2(full)/cc-pVDZ level of theory.

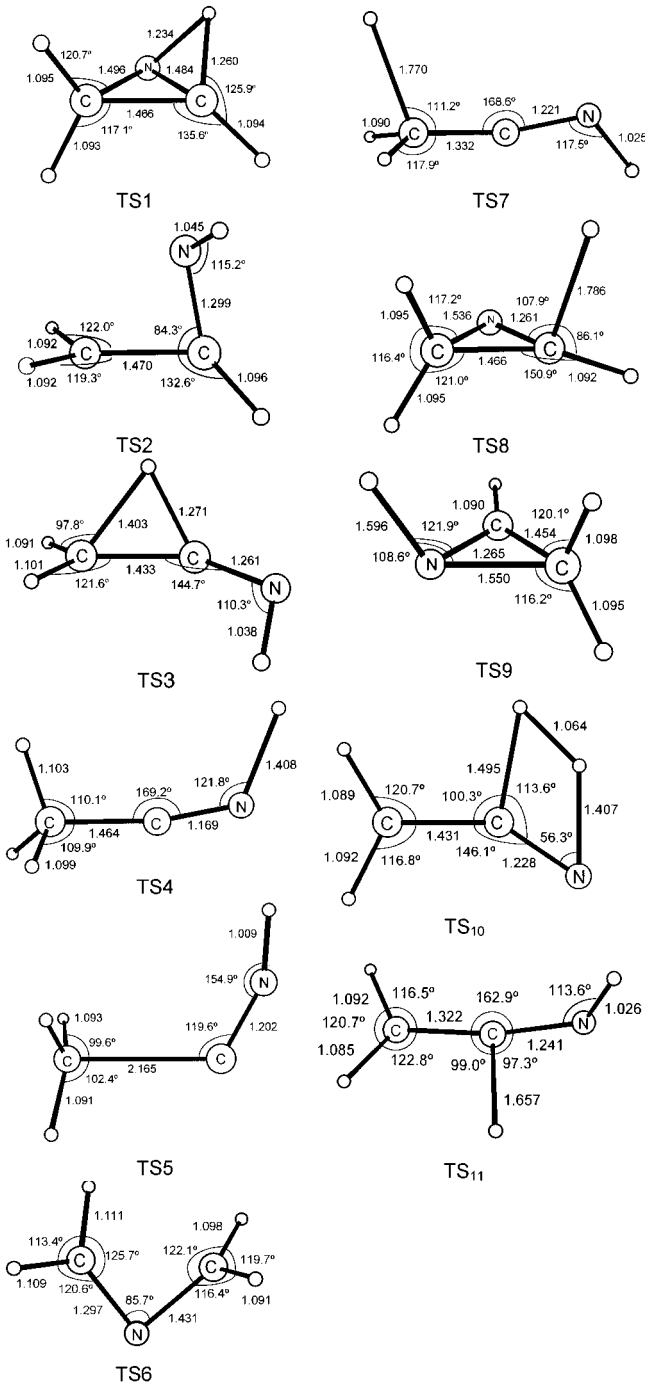

Figure 6. Molecular geometries of the transition states on the lowest doublet potential energy surface for N(^{2}D) + C_2H_4 optimized at the MP2(full)/cc-pVDZ level of theory.

should significantly contribute to the overall rate constants for the reactions of N(^{2}D) with molecules. As mentioned in the Introduction, measurements of the temperature dependence of the rate constants for N(^{2}D) + C_2H_4 and C_2D_4 are currently undertaken by our research group.[15] These experimental data will further contribute to the quantitative estimation of g_e.

B. Reaction Pathways. Figure 4 shows the schematic energy diagram for the lowest doublet potential energy surface of the N(^{2}D) + C_2H_4 reaction. The MP2/cc-pVDZ optimized geometries of intermediates and transition states are shown in Figures 5 and 6, respectively. The total electronic energies of all the species shown in Figure 4 are summarized in Table 3. Table 4 lists the harmonic vibrational frequencies of all the species on

TABLE 3: Total Energies and Symmetry for the Reaction N + C_2H_4 → products

molecule	MP2	PMP4	$\langle S^2 \rangle^a$	symmetry
fragment				
N(^{4}S)		−54.52447	3.756	
N(^{2}D)		−54.43659	1.766	
H(^{2}S)		−0.49981	0.750	
NH($^3\Sigma$)	−55.07219	-55.15230	2.016	$C_{\infty v}$
H_2($^1\Sigma$)	−1.15522	−1.17162	0.000	$D_{\infty h}$
CH_2($^3B_1$)	−39.02178	−39.09111	2.016	C_{2v}
NH_2($^2B_1$)	−55.71297	−55.80694	0.758	C_{2v}
HNC($^1\Sigma$)	−93.14310	−93.28177	0.000	$C_{\infty v}$
CH_3($^2A''$)	−39.69309	−39.77624	0.762	D_{3h}
C_2H_2($^1\Sigma$)	−77.08737	-77.21895	0.000	$D_{\infty h}$
H_2CN($^2B_2$)	−93.69187	−93.85191	0.906	C_{2v}
C_2H_3($^2A'$)	−77.63264	−77.78175	0.926	C_s
CH_2CN($^2B_1$)	−131.69680	−131.91201	0.900	C_{2v}
C_2H_4(^1A_g)	−78.32029	−78.46935	0.000	D_{2h}
CH_2=C=NH($^1A'$)	−132.31423	−132.53026	0.000	C_s
CH_3CN($^1A_1$)	−132.85329	−133.07715	0.000	C_{3v}
c-CH(NH)CH($^1A'$)	−132.22658	−132.44230	0.000	C_s
c-CH (N)CH_2($^1A'$)	−132.28792	−132.49870	0.000	C_s
intermediate				
M_1($^2B_1$)	−132.85329	-133.07715	0.765	C_{2v}
M_2(^2A)	−132.83652	-133.05855	0.760	C_1
M_3(^2A)	−132.85673	-133.08368	0.768	C_1
M_4($^2A'$)	−132.87905	-133.10476	0.800	C_s
M_5($^2A_2$)	−132.86777	-133.10377	0.966	C_{2v}
M_6(^2A)	−132.83943	-133.07140	0.913	C_1
transition state				
TS_1(^2A)	−132.77753	-133.00343	0.803	C_1
TS_2(^2A)	−132.77399	-133.01715	1.138	C_1
TS_3(^2A)	−132.78853	-133.01718	0.807	C_1
TS_4($^2A'$)	−132.83252	-133.06198	0.884	C_s
TS_5($^2A'$)	−132.82087	-133.04878	0.820	C_s
TS_6(^2A)	−132.79017	-133.02910	1.028	C_1
TS_7($^2A'$)	−132.79707	-133.02944	0.912	C_s
TS_8(^2A)	−132.76131	-132.99405	0.969	C_1
TS_9(^2A)	−132.76194	-132.99230	0.939	C_1
TS_{10}($^2A''$)	−132.71215	−132.94867	0.922	C_s
TS_{11}(^2A)	−132.78447	-133.02052	0.920	C_1
TS_{12}($^2A''$)	−132.77898	−133.00842	0.865	C_s
TS_{13}($^2A'$)	−132.77388	−133.02010	0.997	C_s

[a] Expectation value of S^2 calculated at the HF/cc-pVTZ//MP2/cc-pVDZ level of theory.

the potential energy surface calculated at the MP2/cc-pVDZ level of theory. Figure 4 also includes the relative energies obtained from experimental thermochemical data,[23,24] although available experimental data are very limited. Excellent agreements with the experimental data were obtained for the relative energies of N(^{2}D) + C_2H_4 and NH($^3\Sigma$) + C_2H_3. It is seen that the error in the relative energy for the CH_3CN + H products is somewhat large. It can be concluded that the relative energies of the present ab initio calculations are reliable within about 8 kcal/mol.

The cyclic intermediate radical M_1 can be formed by the addition of N(^{2}D) to the CC π-bond in C_2H_4. If the N(^{2}D) atom inserts into the CH bond, the intermediate M_3 is directly produced. However, the latter mechanism may not be important because of its large barrier height as mentioned in the previous section. The intermediate M_1 can isomerize into M_2 or M_5 via the corresponding transition states TS_1 or TS_6. Also, the intermediate M_1 can dissociate into the cyclic-HC(N)CH_2 + H products via the transition state TS_8. It is found that the intermediate M_5 is the most stable intermediate on the doublet potential energy surface at the PMP4 level of theory. This is probably because the intermediate M_5 is isoelectronic with the allyl radical (CH_2CHCH_2) and the electronic structure of M_5 is very similar to that of allyl radical. TS_2 in Figure 4 is the

TABLE 4: Harmonic Vibrational Frequencies Calculated at the MP2/cc-pVDZ Level

molecule	vibrational frequencies/cm^{-1}
fragment	
NH	3343(σ)
H_2	4501(σ)
CH_2	1160(a_1), 3208(a_1), 3442(b_2)
NH_2	1570(a_1), 3418(a_1), 3525(b_2)
HNC	493(π), 2015(σ), 3824(σ)
CH_3	388(a_2''), 1430(e′), 3185(a_1'), 3390(e′)
C_2H_2	561(π), 752(π), 1967(σ), 3459(σ), 3545(σ)
H_2CN	946(b_2), 1150(b_1), 1406(a_1), 2063(a_1), 3075(a_1), 3153(b_2)
C_2H_3	742(a′), 974(a″), 1046(a"), 1092(a′), 1411(a′), 1853(a′), 3160(a′), 270(a′), 3314(a′)
CH_2CN	427(b_2), 453(b_1), 572(b_1), 1033(a_1), 1069(b_2), 1459(a_1), 2760(a_1), 3258(a_1), 3394(b_2)
C_2H_4	826(b_{2u}), 938(b_{2g}), 974(b_{3u}), 1067(a_u), 1236(b_{3g}), 1377(a_g), 1469(b_{1g}), 1690(a_g), 3193(b_{1u}), 3212(a_g), 3291(b_{3g}), 3317(b_{2u})
CH_2═C═NH	404(a″), 462(a′), 678(a′), 910(a″), 996(a″), 1029(a′), 1147(a′), 1436(a′), 2115(a′), 3229(a′), 3341(a″), 3499(a′)
CH_3CN	363(e), 943(a_1), 1058(e), 1410(a_1), 1479(e), 2213(a_1), 3114(a_1), 3221(e)
c-CH(NH)CH	528(a′), 542(a″), 719(a″), 885(a′), 962(a″), 1078(a′), 1159(a″), 1382(a′), 1736(a′), 3336(a″), 3348(a′), 3393(a′)
c-CH(N)CH_2	688(a′), 777(a″), 987(a″), 997(a′), 1031(a′), 1114(a″), 1295(a′), 1504(a′), 1658(a′), 3163(a′), 3271(a″), 3279(a′)
intermediate	
M_1	693(b_1), 853(b_2), 855(a_2), 907(a_1), 1033(b_1), 1064(b_2), 1111(a_1), 1174(a_2), 1277(a_1), 1453(b_2), 1489(a_1), 3164(b_2), 3168(a_1), 3258(a_2), 3274(b_1)
M_2	769, 814, 888, 910, 991, 1075, 1106, 1212, 1236, 1356, 1518, 3161, 3231, 3270, 3510
M_3	437, 667, 723, 932, 981, 1098, 1106, 1187, 1340, 1458, 2696, 3181, 3272, 3332, 3532
M_4	166(a″), 439(a′)672(a″), 875(a′), 967(a′), 1041(a″), 1168(a′), 1374(a′), 1465(a′), 1469(a″), 2391(a′), 3088(a′), 3200(a′), 3212(a″), 3536(a′)
M_5	487(a_1), 499(a_2), 631(b_1), 894(a_2), 915(b_1), 1067(b_2), 1196(b_2), 1208(a_1), 1335(a_1), 1511(b_2), 1586(a_1), 3110(b_2), 3120(a_1), 3292(b_2), 3294(a_1)
M_6	375, 488, 672, 796, 849, 947, 1127, 1262, 1342, 1647, 1899, 3156, 3353, 3563, 3679
transition state	
TS_1	2003i, 727, 839, 907, 955, 1010, 1092, 1117, 1248, 1314, 1526, 2606, 3170, 3234, 3276
TS_2	1525i, 391, 704, 768, 904, 1004, 1112, 1128, 1350, 1470, 1567, 3200, 3215, 3226, 3326
TS_3	1832i, 403, 504, 768, 841, 1002, 1040, 1123, 1306, 1423, 2282, 2627, 3147, 3317, 3341
TS_4	2096i(a′), 123(a″), 316(a′), 478(a″), 665(a′), 978(a′), 1078(a″), 1080(a′), 1403(a′), 1471(a′), 1475()(a″), 2573(a′), 3095(a′), 3199(a′), 3227(a″)
TS_5	565i(a′), 42(a″), 234(a′), 435(a′), 484(a″), 570(a′), 580(a″), 863(a′), 1430(a′), 1440(a″), 1975(a′), 3151(a′), 3329(a″), 3348(a′), 3764(a′)
TS_6	1201i, 535, 679, 820, 1047, 1142, 1173, 1215, 1437, 1501, 1623, 3016, 3103, 3148, 3313
TS_7	1315i(a′), 366(a′), 423(a″), 586(a″), 598(a′), 906(a′), 949(a″), 961(a′), 1068(a″), 1259(a′), 1456(a′), 2334(a′), 3237(a′), 3347(a″), 3552(a′)
TS_8	1442i, 356, 530, 749, 991, 996, 1021, 1045, 1136, 1286, 1512, 1685, 3157, 3264, 3269
TS_9	1676i, 393, 492, 740, 861, 998, 1013, 1059, 1135, 1310, 1510, 1759, 3143, 3254, 3299
TS_{10}	2419i(a′), 355(a″), 395(a″), 502(a′), 573(a″), 831(a″), 944(a′), 1043(a′), 1077(a′), 1432(a′), 1780(a′), 2259(a′), 2595(a′), 3220(a′), 3372(a′)
TS_{11}	1691i, 474, 550, 559, 703, 769, 958, 1031, 1038, 1339, 1524, 2127, 3244, 3377, 3569
TS_{12}	1721i(a′), 109(a″), 615(a″), 813(a′), 1004(a″), 1025(a′), 1120(a″), 1136(a′), 1173(a′), 1429(a′), 1516(a′), 2115(a′), 3176(a′), 3221(a′), 3548(a′)
TS_{13}	878i(a′), 148(a″), 317(a′), 610(a′), 730(a″), 828(a′), 891(a″), 946(a″), 955(a′), 1570(a′), 2221(a′), 3429(a′), 3464(a′), 3540(a″), 3584(a′)

ring-opening transition state connecting the two intermediates, M_2 and M_3.

Although the lowest product channel in Figure 4 is $CH_2CN + H_2$, there exists a large barrier between this channel and the intermediate M_3. The barrier height for this process is calculated to be 76.7 kcal/mol with respect to M_3. This large value is quite reasonable since the dissociation process is four-center hydrogen molecule elimination. We found a reaction pathway to form CH_3 + HNC, although we could not find a direct reaction pathway leading to CH_3 + HCN. According to recent highly accurate ab initio calculations,[25] the barrier height for the isomerization from HNC to HCN is determined to be 33.5 kcal/mol. This means that the isomerization to HCN is energetically possible if enough vibrational energy is partitioned into HNC. The second-lowest product channel is CH_3CN + H and TS_4 is the saddle point interconnecting the intermediate M_4 with CH_3CN + H. If the intermediate M_4 would effectively be produced in the reaction of N(^{2}D) with ethylene, the dominant product channel should be CH_3CN + H since TS_4 is the lowest saddle point on the potential energy surface. However, since the reaction mechanisms are very complicated, it may be very difficult to predict main products only from the energy diagram. Therefore, we have performed RRKM calculations to estimate branching fractions of products under collision-free conditions.

The unimolecular rate constants were calculated by standard RRKM theory[26] with the Whitten−Rabinovich approximation. The total energy was assumed to be the energy of N(^{2}D) + C_2H_4. To estimate the product branching fractions, the kinetic equations were numerically solved with an initial relative concentration of M_1 being unity. Reactions considered in these calculations, the parameters used in the RRKM calculations, and the RRKM rate constants are summarized in Table 5. The product channels, cyclic-CH(NH)CH + H, $H_2CN + CH_2$, and NH + C_2H_3, were ignored since the energy levels for these channels are much larger than other product channels. The relative concentrations of the intermediates (M_1−M_5) and products are plotted as a function of time in Figure 7. It is interesting to note that the main product of the N(^{2}D) + C_2H_4

TABLE 5: Parameters Used in the RRKM Calculations and Resulting RRKM Rate Constants

reaction	k_i	$L^{\ddagger n}$	E^b	$E_0{}^c$	k^d
$M_1 \rightarrow TS_1 \rightarrow M_2$	k_1	4	104.3	43.8	2.40×10^{11}
$M_2 \rightarrow TS_1 \rightarrow M_1$	k_{-1}	1	92.2	31.7	4.73×10^{11}
$M_2 \rightarrow TS_2 \rightarrow M_3$	k_2	1	92.2	23.6	2.91×10^{12}
$M_3 \rightarrow TS_2 \rightarrow M_2$	k_{-2}	1	106.7	38.1	4.61×10^{11}
$M_3 \rightarrow TS_3 \rightarrow M_4$	k_3	1	106.7	37.7	6.48×10^{11}
$M_4 \rightarrow TS_3 \rightarrow M_3$	k_{-3}	3	121.2	52.2	1.22×10^{11}
$M_4 \rightarrow TS_4 \rightarrow CH_3CN + H$	k_4	1	121.2	21.3	1.83×10^{13}
$M_4 \rightarrow TS_5 \rightarrow CH_3 + HNC$	k_5	1	121.2	30.2	2.41×10^{13}
$M_1 \rightarrow TS_6 \rightarrow M_5$	k_6	2	104.3	28.8	1.98×10^{12}
$M_5 \rightarrow TS_6 \rightarrow M_1$	k_{-6}	1	121.9	46.4	6.58×10^{10}
$M_4 \rightarrow TS_7 \rightarrow CH_2{=}C{=}NH + H$	k_7	3	121.2	41.5	2.74×10^{12}
$M_1 \rightarrow TS_8 \rightarrow$ c-CH(N)CH_2 + H	k_8	4	104.3	46.8	7.35×10^{11}
$M_2 \rightarrow TS_9 \rightarrow$ c-CH(N)CH_2 + H	k_9	1	92.2	35.8	1.26×10^{12}
$M_3 \rightarrow TS_{10} \rightarrow CH_2CN + H_2$	k_{10}	1	106.7	76.7	1.91×10^{9}
$M_3 \rightarrow TS_{11} \rightarrow CH_2{=}C{=}NH + H$	k_{11}	1	106.7	32.9	3.94×10^{12}

[a] Statistical factor.[27] [b] Energy of reactant molecule in units of kcal/mol. [c] Barrier height in units of kcal/mol. [d] RRKM rate constant in units of s^{-1} calculated at energy E.

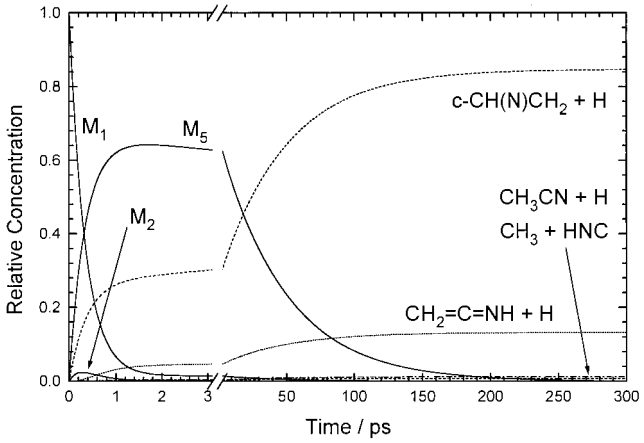

Figure 7. Time profile of relative concentrations of intermediates and products.

reaction is cyclic-CH(N)CH_2 + H, although the energy of this channel is not so low. This is simply because the RRKM rate constant k_8 is larger than k_1. In other words, the intermediate M_1 can dissociate to cyclic-CH(N)CH_2 + H via TS_8 prior to the isomerization via TS_1. Final branching fractions obtained were 0.848, 0.132, 0.012, and 0.008 for cyclic-CH(N)CH_2 + H, CH_2=C=NH + H, CH_3 + HNC, and CH_3CN + H, respectively. The branching fractions for other product channels were almost zero. The branching fraction for CH_2=C=NH + H was calculated to be the second highest. This product is mainly produced from the intermediate M_3 via TS_{11} rather than from M_4 via TS_7 since k_{11} is larger than k_7. It is also interesting to note that the branching fraction to produce CH_3CN + H is slightly smaller than that to produce CH_3 + HNC despite the fact that the barrier height for the former process is smaller than that for the latter process. The reason for this is that the RRKM rate constant k_5 is slightly larger than k_4. Finally, from Figure 7, it can be seen that the lifetime of the intermediate M_5 is very long and is estimated to be about 70 ps.

C. Comparison with Reactions of Other Atoms. It should be interesting to compare the reaction mechanisms of N(2D) + C_2H_4 with reactions between other atoms and C_2H_4. The most extensive studies have been done on the reaction of ground-state oxygen atom O(3P) with ethylene.[28] It has now been established that the O(3P) atom adds to the one of the carbon atoms in C_2H_4 to form a triplet CH_2CH_2O diradical with a barrier. Since a barrier of the isomerization path from CH_2CH_2O to a triplet acetaldehyde CH_3CHO is very large, the main exit channel is the C−H dissociation of the triplet CH_2CH_2O diradical to produce CH_2CHO + H. This process can be viewed as an oxygen−hydrogen exchange. In the case of N(2D) + C_2H_4, the overall main process can also be viewed as a nitrogen−hydrogen exchange since the main exit channel is predicted to be cyclic-CH(N)CH + H from the RRKM calculations.

Compared with the extensive studies on the reaction of O(3P), there have been few reports on the O(1D) + C_2H_4, in which the reaction products are directly detected. Honma[29] has reported vibrational and rotational distributions of OH and concluded that O(1D) primarily inserts into a CH bond of ethylene and OH is produced via elimination from an intermediate. If insertion were a dominant mechanism, there would be a large difference between the reactions of O(1D) and N(2D) with C_2H_4.

Very recently, crossed-beam experiments have been carried out for the reaction between ground-state carbon atoms C(3P) and ethylene.[30] An initial step of this reaction is the addition of C to the ethylene π-bond to form cyclopropylidene (cyclic-CH_2(C)CH_2). Therefore, the reaction mechanism is very similar to the N(2D) reaction, although the main product of C(3P) + C_2H_4 has been reported to be a propagyl radical $CH_2C{\equiv}CH$, which is produced via a subsequent ring-opening process. Soon it will be possible to discuss similarity and difference in the detailed dynamics between these two reactions since the cross-beam experiments are currently undertaken.[11]

Conclusion

The lowest doublet potential energy surface for the reaction of N(2D) with C_2H_4 has been characterized at two different ab initio levels of theory. The CASSCF calculations have been carried out in order to understand whether the reaction is additive or insertive. The transition state geometries for both mechanisms were optimized at the CASSCF/cc-pVDZ level. It has been found that the barrier height for the addition of N(2D) to the CC π-bond in C_2H_4 is smaller than that for the insertion of N(2D) into the CH bond in C_2H_4. Conventional TST calculations have been performed by using the saddle point properties calculated at the CASSCF/cc-pVDZ level and compared to the experimental rate constant although only the rate constant at room temperature is available. A serious disagreement has been found, and we qualitatively conclude that nonadiabatic transitions play an important role on the absolute values of the rate constants. The reaction pathways have been discussed on the basis of the PMP4(SDTQ)/cc-pVTZ//MP2/cc-pVDZ level calculations. Five intermediates and eleven transition states have been found on the potential energy surface for the N(2D) + C_2H_4 reaction. It is predicted that cyclic-CH(N)CH_2 is mainly produced in the N(2D) + C_2H_4 reaction from simple RRKM calculations under collision-free conditions. Further experimental studies such as direct detection of the reaction products will be necessary to confirm the theoretical results presented in this paper.

Acknowledgment. T.T. thanks Professor P. Casavecchia for many informative conversations and e-mail communications.

References and Notes

(1) Brocklehurst, B.; Jennings, K. R. *Prog. React. Kinet.* **1967**, *4*, 1.
(2) Safrany, D. R. *Prog. React. Kinet.* **1971**, *6*, 1.
(3) Fell, B.; Rivas, I. V.; McFadden, D. L. *J. Phys. Chem.* **1981**, *85*, 224.
(4) Umemoto, H.; Sugiyama, K.; Tsunashima, S.; Sato, S. *Bull. Chem. Soc. Jpn.* **1985**, *58*, 3076.
(5) Umemoto, H.; Matsumoto, K. *J. Chem. Soc., Faraday, Trans.* **1996**, *92*, 1315.
(6) Umemoto, H.; Asai, T.; Kimura, Y. *J. Chem. Phys.* **1997**, *106*, 4985.

(7) Umemoto, H.; Kimura, Y.; Asai, T. *Chem. Phys. Lett*. **1997**, *264*, 215.

(8) Umemoto, H.; Kimura, Y.; Asai, T. *Bull. Chem. Soc. Jpn*. **1997**, *70*, 2951.

(9) Alagia, M.; Aquilanti, V.; Ascenzi, D.; Balucani, N.; Cappelletti, D.; Cartechini, L.; Casavecchia, P.; Pirani, F.; Sanchini, G.; Volpi, G. G. *Israel J. Chem*. **1997**, *37*, 329.

(10) Alagia, M.; Balucani, N.; Cartchini, L.; Casavecchia, P.; Volpi, G. G.; Takayanagi, T.; Kurosaki, Y. Submitted for publication.

(11) Casavecchia, P. Private communication.

(12) Kobayashi, H.; Takayanagi, T.; Yokoyama, K.; Sato, T.; Tsunashima, S. *J. Chem. Soc., Faraday Trans*. **1995**, *91*, 3771.

(13) Kurosaki, Y.; Takayanagi, T.; Sato, K.; Tsunashima, S. *J. Phys. Chem.* **1998**, *102*, 254.

(14) Takayanagi, T.; Kurosaki, Y.; Misawa, K.; Sugiura, M.; Kobayashi, Y.; Sato, K.; Tsunashima, S. *J. Phys. Chem*. **1998**, *102*, 6251.

(15) Tsunashima, S.; Sato, K.; Takayanagi, T.; Kurosaki, Y. To be published.

(16) Frisch, M. J.; Trucks, G. W.; Schlegel, H. B.; Gill, P. M. W.; Johnson, B. G.; Robb, M. A.; Cheeseman, J. R.; Keith, T.; Petersson, G. A.; Montgomery, J. A.; Raghavachari, K.; Al-Laham, M. A.; Zakrzewski, V. G.; Ortiz, J. V.; Foresman, J. B.; Cioslowski, J.; Stefanov, B. B.; Nanayakkara, A.; Challacombe, M. C.; Peng, Y.; Ayala, P. Y.; Chen, W.; Wong, M. W.; Andres, J. L.; Replogle, E. S.; Gomperts, R.; Martin, R. L.; Fox, D. J.; Binkley, J. S.; Defrees, D. J.; Baker, J.; Stewart, J. P.; Head-Gordon, M.; Gonzalez, C.; Pople, J. A. *Gaussian 94*; Gaussian, Inc.: Pittsburgh, PA, 1995.

(17) Dunning, T. H., Jr. *J. Chem. Phys*. **1989**, *90*, 1007.

(18) Soto, M. R.; Page, M. *J. Chem. Phys*. **1992**, *97*, 7287.

(19) McDouall, J. J.; Peasley, K.; Robb, M. A. *Chem. Phys. Lett*. **1988**, *148*, 183.

(20) Truhlar, D. G. *J. Chem. Phys*. **1972**, *56*, 3189.

(21) Muckerman, J. T.; Newton, M. D. *J. Chem. Phys*. **1972**, *56*, 3191.

(22) Bunker, D. L. *J. Chem. Phys*. **1960**, *32*, 1001.

(23) *JANAF Thermochemical Tables*, 3rd ed.; Natl. Stand. Ref. Data Ser. (U.S. National Bureau of Standards, U.S. Government Printing Office: Washington, DC, 1985.

(24) Afeefy, H. Y.; Liebman, J. F.; Stein, S. E. Neutral Thermochemical Data. In *NIST Chemistry WebBook*, NIST Standard Reference Database Number 69; Mallard, W. G., Eds.; Linstrom, P. J., March 1998, National Institute of Standards and Technology, Gaithersburg MD, 20899 (http://webbook.nist.gov).

(25) Holbrook, A.; Pilling, M. J.; Robertson, S. H. *Unimolecular Reactions*; John Wiley: Chichester, 1996.

(26) Bowman, J. M.; Gazdy, B.; Bentley, J. A.; Lee, T. J.; Dateo, C. E. *J. Chem. Phys*. **1993**, *99*, 308.

(27) Bishop, D. M.; Laidler, K. J. *Trans. Faraday Soc*. **1970**, *66*, 1685.

(28) For example, Schmoltner, A. M.; Chu, P. M.; Brudzynski, R. J.; Lee, Y. T. *J. Chem. Phys*. **1989**, *91*, 6926.

(29) Honma, K. *J. Chem. Phys*. **1993**, *99*, 7677.

(30) Kaiser, R. I.; Lee. Y. T.; Suits, A. G. *J. Chem. Phys*. **1996**, *105*, 8705.